Composites: Part A 86 (2016) 66–76

Contents lists available at ScienceDirect

Composites: Part A

journal homepage: www.elsevier.com/locate/compositesa

Detection of fibre fracture and ply fragmentation in thin-ply UD carbon/glass hybrid laminates using acoustic emission

Mohamad Fotouhi [a,b,*], Putu Suwarta [b], Meisam Jalalvand [b], Gergely Czel [c,b], Michael R. Wisnom [b]

[a] Non-destructive Testing Lab, Department of Mechanical Engineering, Amirkabir University of Technology, 424 Hafez Ave, 15914 Tehran, Iran
[b] Advanced Composites Centre for Innovation and Science, University of Bristol, Bristol BS8 1TR, UK
[c] MTA–BME Research Group for Composite Science and Technology, Budapest University of Technology and Economics, Műegyetem rkp. 3, H-1111 Budapest, Hungary

ARTICLE INFO

Article history:
Received 29 January 2016
Received in revised form 30 March 2016
Accepted 3 April 2016
Available online 4 April 2016

Keywords:
A. Hybrid
A. Laminates
B. Fragmentation
D. Acoustic emission

ABSTRACT

This paper investigates the link between acoustic emission (AE) events and the corresponding damage modes in thin-ply UD carbon/glass hybrid laminates under tensile loading. A novel configuration was investigated which has not previously been studied by AE, where the laminates were fabricated by embedding thin carbon plies between standard thickness translucent glass plies to produce progressive fragmentation of the carbon layer and delamination of the carbon/glass interface. A criterion based on amplitude and energy of the AE event values was established to identify the fragmentation failure mode. Since the glass layer was translucent, it was possible to quantitatively correlate the observed fragmentation during the tests and the AE events with high amplitude and energy values. This new method can be used as a simple and advanced tool to identify fibre fracture as well as estimate the number and sequence of damage events that are not visible e.g. in hybrid laminates with thick or non-transparent layers as well as when the damage is too small to be visually detected.

1. Introduction

Hybridisation of different continuous uni-directional (UD) prepregs is a successful method to address the lack of ductility in composite laminates. Hybrid composites usually consist of two different fibres and in many previous works, carbon and glass layers were the constituents [1–6].

Recently, gradual failure and pseudo-ductile stress–strain response in thin carbon/glass plies were observed by Czél and Wisnom [7–9] and Jalalvand et al. [10]. Their results showed that as the failure strain of carbon fibres is lower than that of the glass fibres, the first damage occurs in the carbon layer and the following failure mechanisms in the specimen are influenced by the interfacial toughness, material properties, and the thickness of the layers. It was reported that when the carbon layer was thin enough, catastrophic delamination propagation following the first carbon layer fracture was suppressed and further fractures in the carbon layer occurred. This damage mode was called fragmentation of the carbon layer. In another study by Jalalvand et al. [11,12] the effect of the configuration parameters on damage evolution in UD carbon/S-glass interlayer hybrids was investigated by means of novel damage mode maps. Using the damage mode map concept, they were able to easily predict the failure modes in the different hybrid configurations and find the optimal UD hybrid configuration for maximum pseudo-ductility. In those studies, it was observed and predicted with both numerical and analytical modelling tools that the damage modes causing pseudo-ductile behaviour in thin-ply UD carbon/S-Glass interlaminar hybrid laminates are carbon ply fragmentation and delamination of the carbon/glass interface.

Understanding the failure mechanisms which have introduced pseudo-ductility is of importance for the optimal use of a component and can then be applied in designing more general layups with gradual failure. But the characterisation of these damage mechanisms is a challenging issue, mostly in the following cases where the different damage modes are not visible.

(1) In laminates which are not transparent; for example those with carbon plies on the surface [13] or the epoxy matrix in glass prepreg modified with carbon nano-particles.
(2) When the laminate is too thick to observe the failure modes through the transparent material, or it is has been made with several multi-directional layers such as quasi-isotropic laminates.

* Corresponding author at: Non-destructive Testing Lab, Department of Mechanical Engineering, Amirkabir University of Technology, 424 Hafez Ave, 15914 Tehran, Iran.
E-mail address: fotouhi.mohamad@gmail.com (M. Fotouhi).

http://dx.doi.org/10.1016/j.compositesa.2016.04.003
1359-835X/

Table 1
Characteristics of the prepregs and fibres used.

Prepreg type	S-glass/ epoxy	TR30/ epoxy	MR40/ epoxy
Fibre modulus E (GPa)	88	234	295
Fibre failure strain (%)	5.5	1.9	1.5
Cured nominal thickness (mm)	0.155	0.029	0.061
Fibre mass per unit area (g/m^2)	190	21.2	50
Fibre volume fraction (%)	50	41	45

(3) When there is a mixture of failure modes taking place simultaneously and it is hard to distinguish them visually.

This study proposes an efficient method to investigate damage development and to identify the type of damage in thin-ply UD carbon/glass hybrid laminates using AE technique. AE registration is an efficient method for monitoring and recording damage in-situ and on-line during loading of a structure. Compared with other non-destructive methods, AE has the advantage of continuous monitoring of structures [14]. AE signals originate from the sudden release of strain energy due to damage formation inside the material.

Many studies have sought to establish correlation between the damage mechanisms in laminated composite materials and parameters of the AE signals. Several researchers tried to correlate AE parameters to the damage caused, and it was concluded that the amplitude, energy and frequency ranges of different damage modes were different from each other [15–27]. High ranges of amplitude, energy and frequency of AE signals were usually associated with fibre failure, middle ranges with delamination/debonding and low ranges with transverse/longitudinal matrix cracking. In some studies the frequency was found to be a good AE parameter to separate the damage modes [15–19], in other studies amplitude or energy of AE signals were used for damage classification [20–26]. Cumulative AE count and AE energy curves were used by previous researchers for identification of thresholds of the damage evolution during loading [27–29]. Other researchers have shown that a single characteristic of the AE signals is often not enough to discriminate the different damage mechanisms. As a result, multivariable analysis tools, such as fuzzy c-means clustering and genetic algorithms, have been used to successfully classify the AE signals corresponding to different failure modes [30–39].

The literature review indicates that AE technique can characterise the damage modes in laminated composites and it had some applicability mostly for identification of thresholds of the damage development in hybrid laminates. However, the applicability of AE technique in complex loading cases and hybrid laminates remains a hypothesis not proven by direct observation.

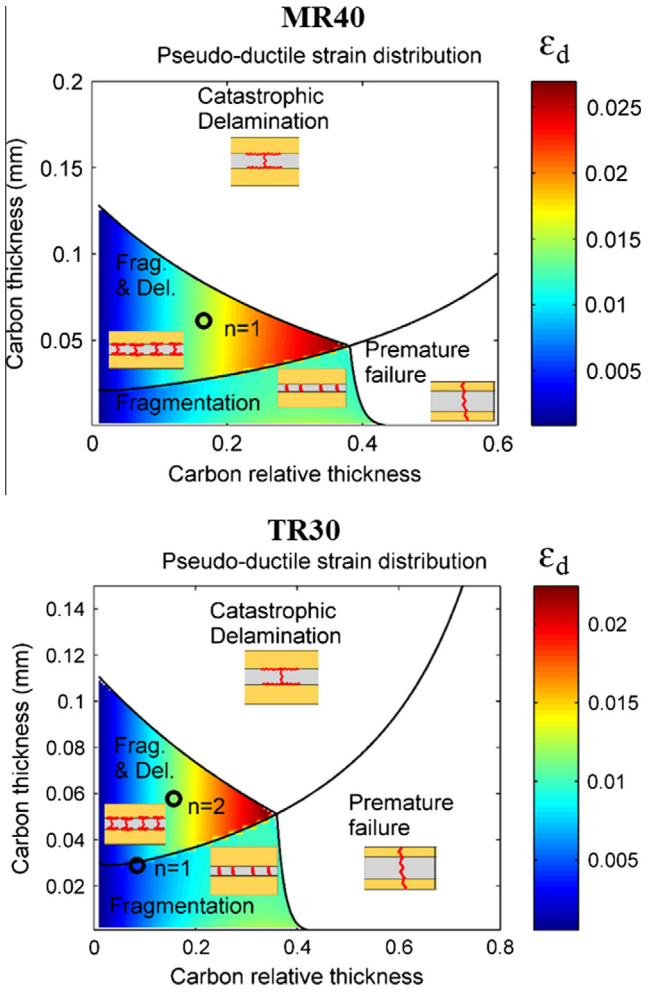

Fig. 2. Distribution of pseudo-ductile strain for [$G_1/C_n/G_1$] laminates made with MR40 and TR30 carbon, where (n = 1–3). (For interpretation of the references to colour in this figure legend, the reader is referred to the web version of this article.)

The aim of this study is to establish a direct correlation between the observed damage mechanisms and the recorded AE signals in UD carbon/S-glass hybrid laminates under tensile loading. To achieve this goal, thin-ply hybrid materials were investigated in which progressive fragmentation of the carbon/epoxy layer and stable delamination of the carbon/glass interface were the main failure modes.

The investigated layups allow multiple ply fragmentation to be quantitatively assessed, which has not previously been possible

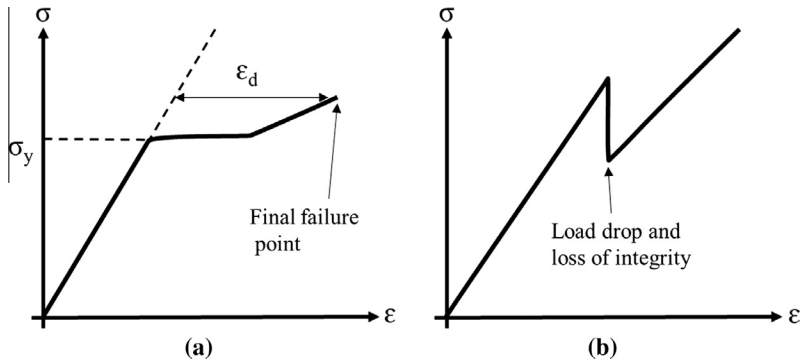

Fig. 1. Schematic of the typical stress–strain graph of (a) a thin-ply hybrid with pseudo-ductility and (b) a conventional hybrid with catastrophic delamination.

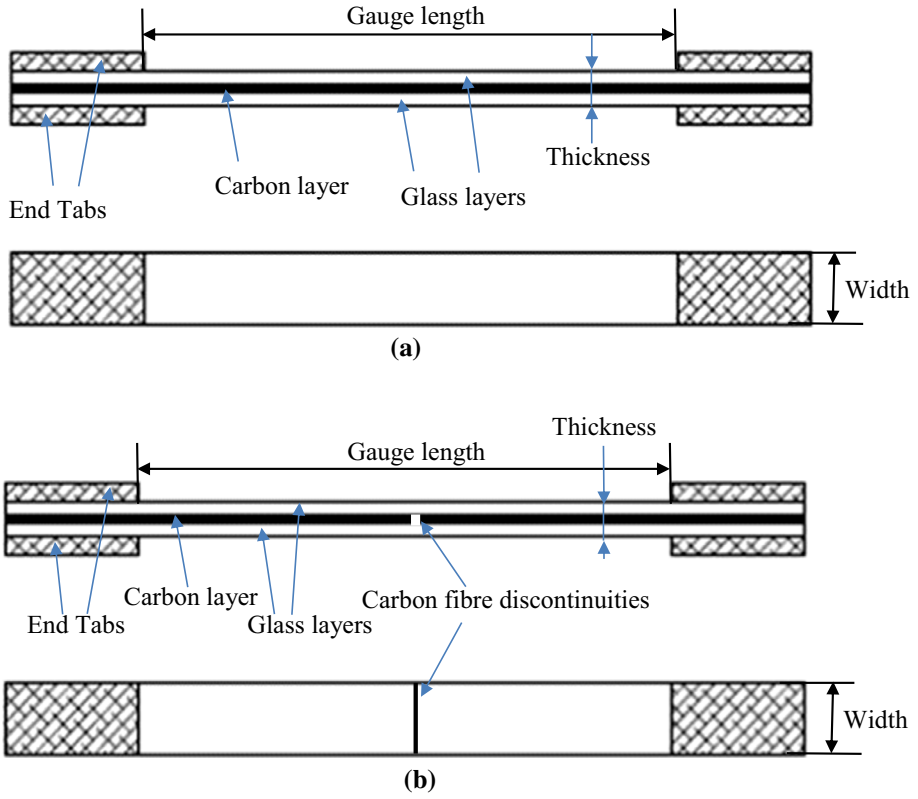

Fig. 3. Schematics of thin ply hybrid composite specimen types for tensile testing with (a) continuous and (b) pre-cut carbon layers. (For interpretation of the references to colour in this figure legend, the reader is referred to the web version of this article.)

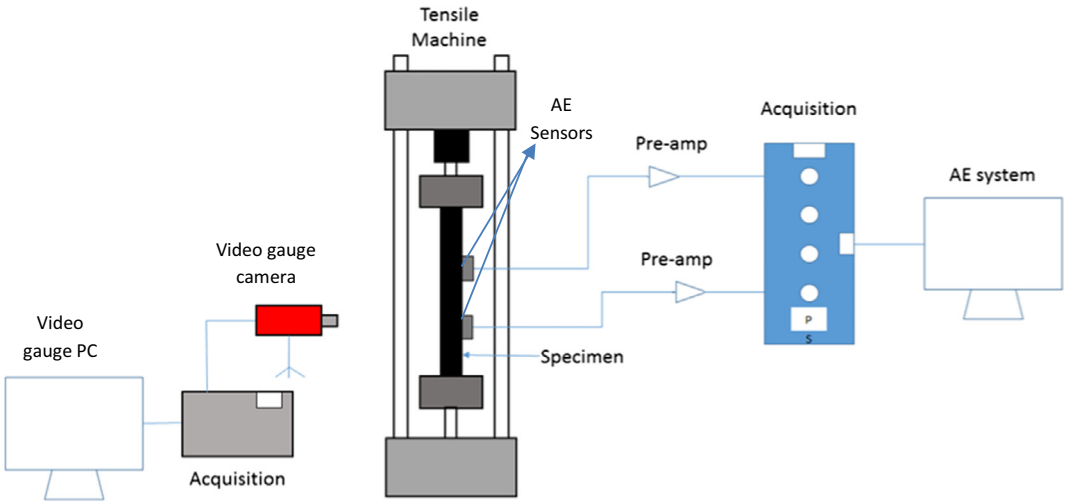

Fig. 4. Schematic of the experimental setup. (For interpretation of the references to colour in this figure legend, the reader is referred to the web version of this article.)

because fibre direction tensile failure is normally sudden and catastrophic. Since the glass/epoxy surface ply was translucent, it was possible to observe the failure modes and to correlate the AE signals registered during the tensile loading to the actual damage accumulation. There were two main failure modes, i.e. ply fragmentation and carbon/glass interface delamination. In order to identify and separate AE signals originating from the failure modes, AE characteristics of a mode II stable delamination were obtained by producing pure carbon/glass interface delamination. This was done by inserting a pre-cut in the carbon layer. By knowing the characteristics of the AE events corresponding to pure delamination and ply fragmentation, the obtained AE signals were then classified into two categories with low and high AE energy and amplitude of the AE signal. It was found that AE technique was capable to identify the type of damage. Therefore this technique can be used as an effective method for accurately detection of fibre fragmentation, as well as subsequent tracking of its evolution and accumulation in more complex layups and loading cases.

2. Experiments

2.1. Materials

The materials considered in this study were thin carbon/epoxy prepreg and conventional standard thickness glass/epoxy prepreg. Characteristics of the prepregs are listed in Table 1. The high strain

material of the hybrid laminates is UD S-glass/913 epoxy prepreg supplied by Hexcel. The low strain materials were two types of thin carbon prepregs from SK Chemicals (South Korea) under the trade name of SkyFlex USN020A and SkyFlex UIN050A. The carbon fibres in the thin USN020A and UIN050A prepregs were Pyrofil TR 30 and MR40 respectively both made by Mitsubishi Rayon with the modulus and fibre failure strain given in Table 1. The corresponding matrix was SK Chemical's type K50 epoxy resin. The maximum cure temperature of both S-glass/epoxy and carbon/epoxy layers were 120 °C so they are assumed to be fairly compatible. Although no details were provided by the suppliers on the chemical formulation of the resins, good integrity of the hybrid laminates was confirmed during test procedures and no phase separation was observed on cross sectional micrographs.

2.2. Specimen design

The benefit of using glass prepreg was that it is translucent, allowing crack and delamination detection visually. The hybrid plates were laid up in the following sequence: $[G_1/C_n/G_1]$ where G stands for S-glass plies and C for TR30 or MR 40 carbon plies.

The values of n were chosen based on the previously developed damage mode maps [10,11], to achieve pseudo-ductility through carbon layer fragmentation and dispersed delamination (see Fig. 1a) and avoid catastrophic failure or a stress–strain curve with a significant load drop (Fig. 1b). The pseudo-ductile strain (ε_d), as shown in Fig. 1a, is defined here as the extra strain between the final failure point and the initial slope line at the failure stress level as shown in Fig. 1a. As there is not much damage and nonlinearity before the carbon layer failure, the initial modulus of the hybrid laminate can be easily measured by the slope of a straight line from the origin on the initial linear-elastic part of the stress–strain curve.

Fragmentation in the carbon layer, failure of the glass layer and delamination at the carbon/glass interfaces are the three possible damage modes which compete with each other and whichever has the lower required stress, happens before the others. Since characterisation of different damage types was the aim of this paper, the lay-ups were chosen in a way to have a combination of damage modes, i.e. both fragmentation in the carbon layer and delamination.

In our previous study, the effect of the relative and absolute carbon layer thickness was investigated and described by means of novel Damage Mode Maps [12].

Different possible failure modes for different relative and absolute carbon layer thicknesses are illustrated by the Damage Mode Map for S-glass/TR30 and S-glass/MR40 hybrids in Fig. 2.

The damage mode maps show that $n = 1$ for MR40 and $n = 2$ for TR30 carbon configurations result in the combined fragmentation and dispersed delamination failure mode, whereas $n = 1$ for TR30 carbon configuration is on the border of the pure fragmentation and the combination of fragmentation and dispersed delamination (see Fig. 2a and b). All these three these configurations were chosen for the investigation. The reason for choosing the different configurations was to produce different numbers of events and sizes of damage and to verify the applicability of the AE identification method over a wider area. The hybrid specimen types will be referred to as MR40, 1TR30 and 2TR30. The first number in 1TR30 and 2TR30 refers to the number of carbon plies in the central layer.

In addition, a UD $[G_4/C_8/G_4]$ configuration which has a pre-cut perpendicular to the fibre direction in the TR30 carbon layer, was selected to achieve pure delamination under tensile loading. The cut was across the entire width and thickness of the specimen. With this configuration, delamination initiates at a strain lower than carbon layer failure strain and therefore a stable pure mode II delamination will propagates without any carbon layer fracture. Schematics of the investigated specimen types without and with cut are shown in Fig. 3.

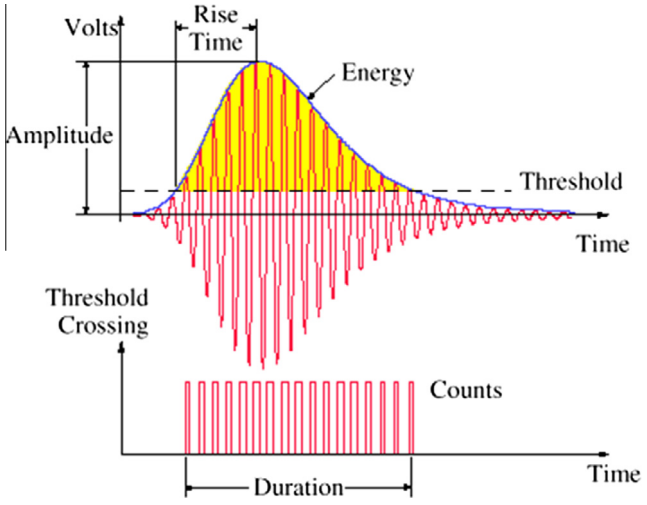

Fig. 5. The definitions for acoustic-emission parameters [37]. (For interpretation of the references to colour in this figure legend, the reader is referred to the web version of this article.)

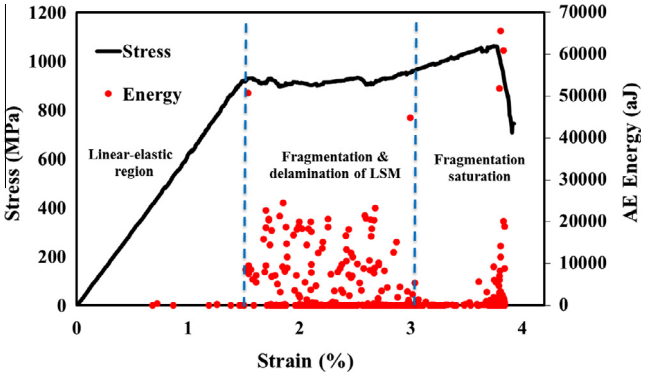

Fig. 6. Stress–strain and AE event energy distribution for a typical MR40/S-glass type specimen. (For interpretation of the references to colour in this figure legend, the reader is referred to the web version of this article.)

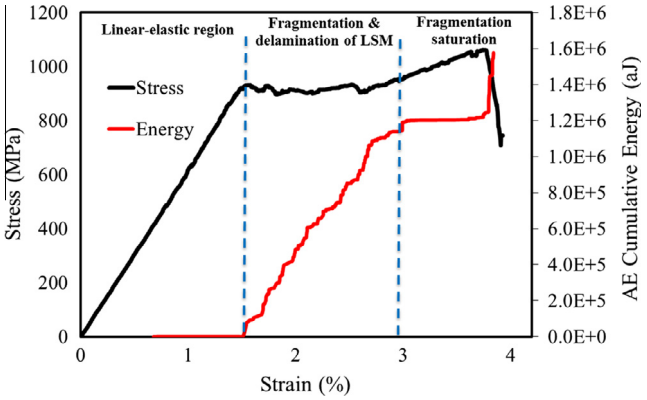

Fig. 7. Stress–strain and cumulative AE energy distribution for a typical MR40/S-glass hybrid specimen. (For interpretation of the references to colour in this figure legend, the reader is referred to the web version of this article.)

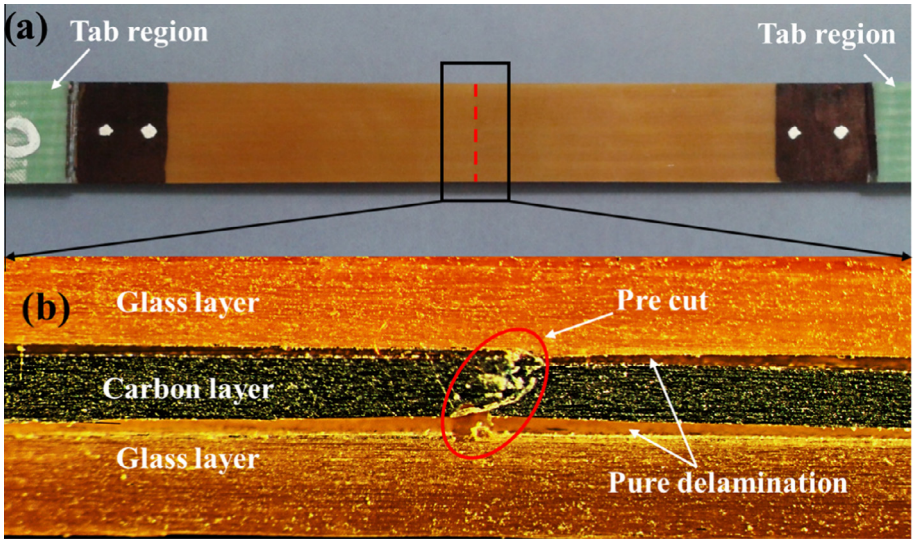

Fig. 8. (a) Top and (b) side view of a typical delaminated [$G_4/C_8/G_4$] type specimen with TR30 carbon. (For interpretation of the references to colour in this figure legend, the reader is referred to the web version of this article.)

2.3. Specimen manufacturing

The laminates were cured in an autoclave at the recommended cure temperature and pressure cycle for the Hexcel 913 resin (60 min@125 °C, 0.7 MPa). Fabrication of the specimens was done using a diamond cutting wheel. End tabs made of 2 mm thick woven glass/epoxy plates supplied by Heathcotes Co. Ltd. were bonded to the specimens using a two component Araldite 2000 A/B epoxy adhesive supplied by Huntsman. The components were mixed with the volume fraction ratio of 100:50 for A:B respectively and cured for 120 min @ 80 °C inside a fan convection oven.

2.4. Test procedure

Tensile testing of the hybrid laminates was executed under uniaxial loading and displacement control using a crosshead speed of 2 mm/min on a computer controlled Instron 8801 type 100 kN rated universal hydraulic test machine with wedge type hydraulic grips. A 25 kN load cell was attached for better resolution in the expected load range. The nominal specimen dimensions for the tests were 240/160/20/h mm overall length/free length/width/-variable thickness respectively. At least 6 specimens of each type were tested. To measure the strains with a nominal gauge length of 130 mm, an Imetrum video gauge system was used, tracking the points applied on the specimen face using points over a particular gauge length. Two AE sensors were located at a distance of 100 mm apart at the middle of the back side of the specimen, to monitor the damage events.

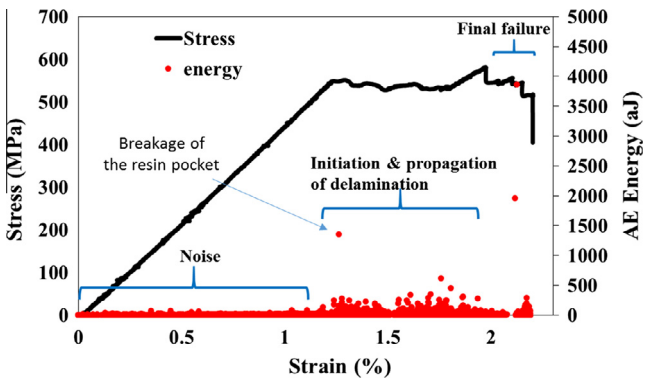

Fig. 9. Stress–strain and AE event energy for pure delamination in a typical [$G_4/C_8/G_4$] with a pre-cut in the TR30 carbon layer. (For interpretation of the references to colour in this figure legend, the reader is referred to the web version of this article.)

2.5. AE device

An AE data acquisition system (PAC) PCI-2 with a maximum sampling rate of 40 MHz was used to record the AE signals. PAC R15 resonant-type, broadband, single-crystal piezoelectric transducers were used as AE sensors. The frequency range of the sensors was 20–900 kHz, and the gain selector of the preamplifier and the threshold value were set to 40 dB. The surface of the sensor was covered with silicon grease to provide good acoustic coupling between the specimen and the sensor. The test sampling rate was 5 MHz. A pencil lead break procedure was used to calibrate the data acquisition system for each of the specimens. After the calibration step, the AE signals were recorded during the tests as illustrated in Fig. 4. Schematic definition of the features of an AE signal such as duration, rise time, amplitude, energy and count are presented in Fig. 5.

3. Results and discussion

3.1. UD hybrid AE results

Tensile testing with simultaneous AE monitoring provides useful information about different aspects of the damage evolution in the hybrid composite specimens. A typical stress–strain plot and its relationship with AE energy is shown in Fig. 6, for a typical MR40/S-glass hybrid specimen. Different types of AE signals were recorded and the first significant AE events were detected at the beginning of the plateau. AE events with different energy levels can be observed for different damage evolution stages in Fig. 6. More detailed discussion of these differences is given in Section 3.2.

The cumulative value of the AE energy is a suitable parameter to represent the overall state and integrity of the specimens. This is illustrated in Fig. 7 for the same MR40/S-glass specimen.

To analyse the AE events during the test, the stress–strain plot is divided into three different regions as follows (see Figs. 6 and 7):

(1) *Before damage initiation:* At the early stage of the loading process and before damage initiation, some weak AE events were detected. These events might be related to some micro-scale damage around the edges of the sample e.g. single fibres coming off the edge and/or grip rubbing effects, so they are believed not to have a considerable effect on the specimen's integrity. In this stage, the tensile strain was lower than the carbon fibre failure strain and the appearance of the specimen did not change.
(2) *Fragmentation & delamination of the carbon layer:* The first significant AE signals and therefore significant rise in the cumulative AE energy diagram were detected in this regime corresponding to the onset of macroscopic damage. It was observed that the fragmentation and significant rise in the cumulative AE energy occurred at the same time. The specimen's appearance also changed from fully black to a tiger striped pattern. This means that the obtained AE signals that appeared in this region were due to fragmentation and dispersed delamination. The observed damage modes agreed with the expectations from the damage mode maps.
(3) *Fragmentation saturation:* In this stage, fragmentation was fully saturated, the contribution of the carbon layer to the specimen stiffness was degraded and the glass layer carried most of the load, with the carbon layer making a negligible contribution. As shown in Figs. 6 and 7, the detected AE signals before close to the final failure were diminished in this regime which means that there was no significant damage in until final fracture of the glass layer. At the end of this stage some significant AE signals were received corresponding to the glass layer fracture. Due to the fragmentation of the carbon layer in the previous stage, the modulus of the specimen became significantly lower than that in the first regime.

In the following section we aimed at characterising the observed failure modes based on their resultant AE event features and correlating them to the visual changes of the specimens' appearance.

3.2. Classification of the damage modes based on visual assessment and AE signals

It was visually observed that the dominant damage modes in the investigated hybrid laminates are a combination of fragmentation and delamination. The observed damage modes were in agreement with the damage mode maps presented in Section 2.2. The

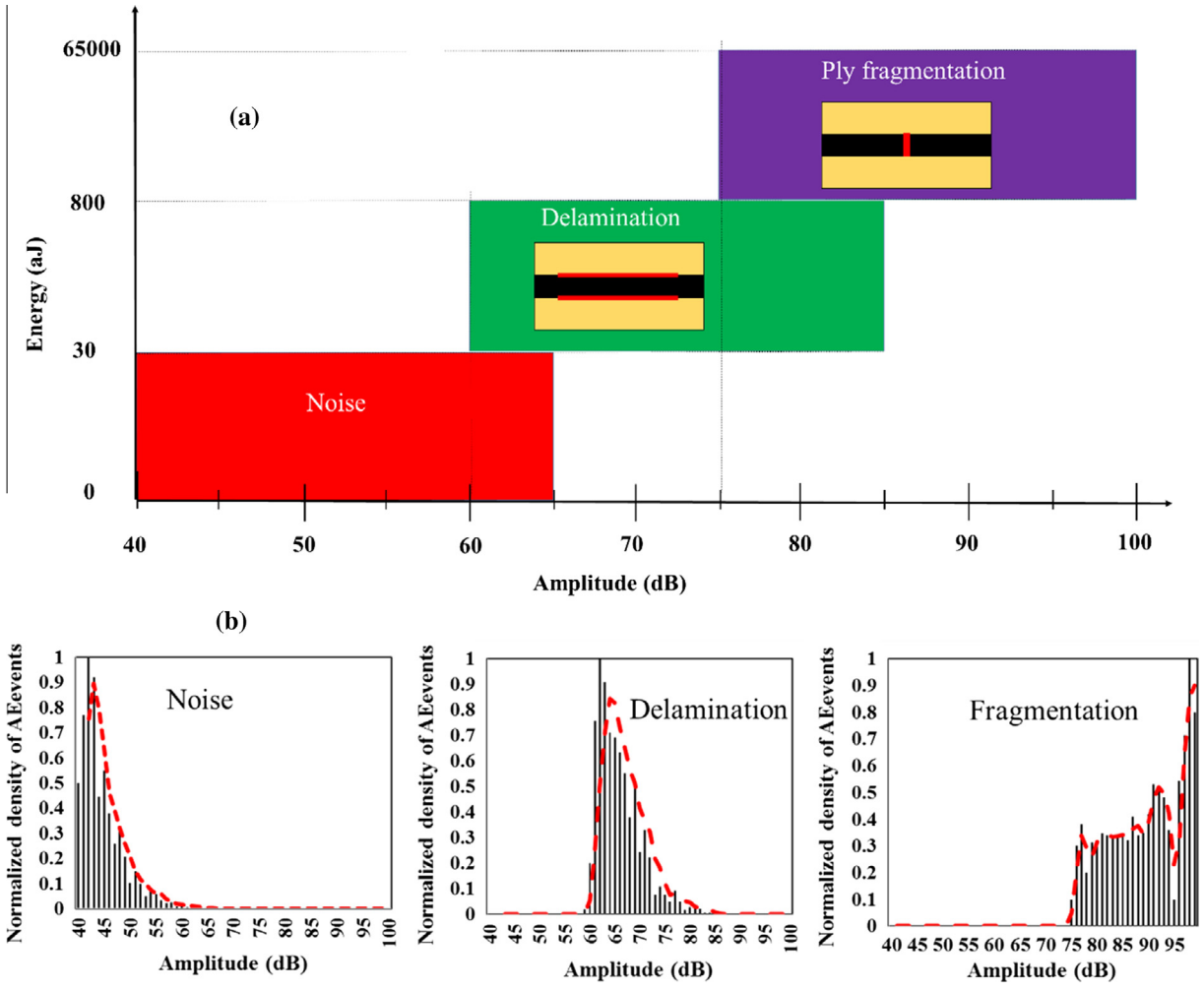

Fig. 10. (a) Event amplitude and energy ranges assigned to different damage mechanisms of ply fragmentation and delamination and (b) density of the AE events in the amplitude domain for a typical MR40 hybrid specimen (the red dash lines are moving average trend lines). (For interpretation of the references to colour in this figure legend, the reader is referred to the web version of this article.)

aim of this section is to identify the fragmentation and delamination damage modes using the AE signals. A large body of literature can be found on AE amplitude or energy based classification of failure mechanisms in laminated composite materials [20–26]. Their results revealed different amplitude and energy ranges for the failure modes observed. It was found that high amplitude and high energy signals are associated with ply fragmentation, and lower ranges with delamination and matrix cracking.

In order to pure delamination, a $[G_4/C_8/G_4]$ laminate with a precut in the carbon layer was utilised. This is a simple tensile test on a specially designed UD hybrid composite specimen showing stable mode II crack propagation due to the presence of the cut in the middle of the central carbon layer. The top and side view of a typical delaminated specimen are shown in Fig. 8.

There is no carbon layer fracture/fragmentation in this specimen since delamination initiates at strains lower than the carbon fibre failure strain. There were likely some isolated single fibre fractures before the initiation of the delamination which did not produce significant AE signals. Therefore, the AE signals in this special specimen type mainly originate from delamination. The stress–strain plot and the energy of the AE signals obtained from delamination are shown in Fig. 9.

The amplitude of the AE signals was between 60 and 75 dB while the event energy was between 30 and 800 aJ for delamination. As highlighted in the figure, there was one single strong AE energy event appearing at the early stage of the test which is believed to correspond to the breakage of the resin pocket at the

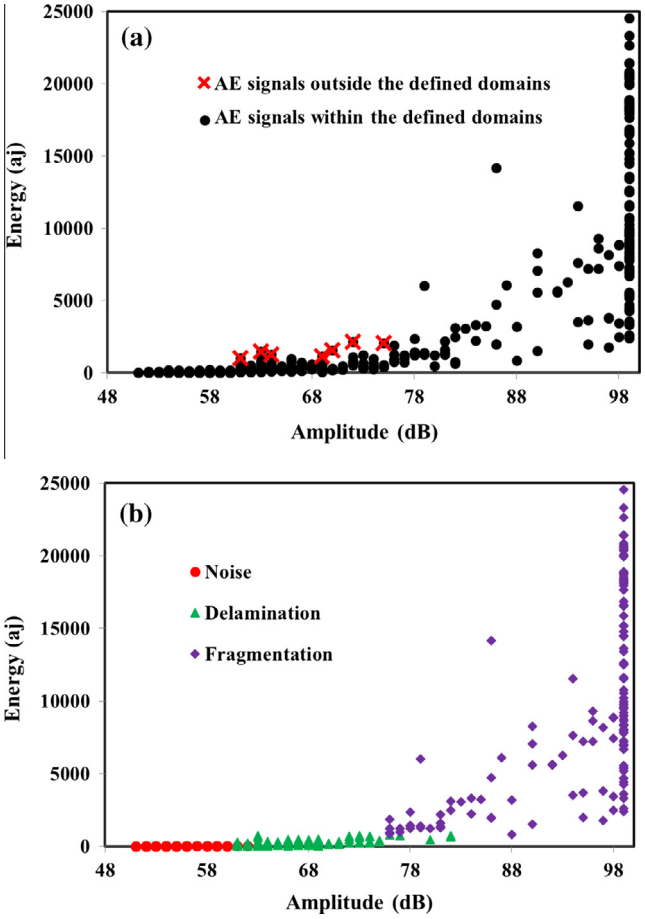

Fig. 11. Plots of amplitude and energy of the AE events for a typical MR40/S-glass specimen. (a) Before applying the defined boundaries in Fig. 10a. (b) After applying the defined boundaries. (For interpretation of the references to colour in this figure legend, the reader is referred to the web version of this article.)

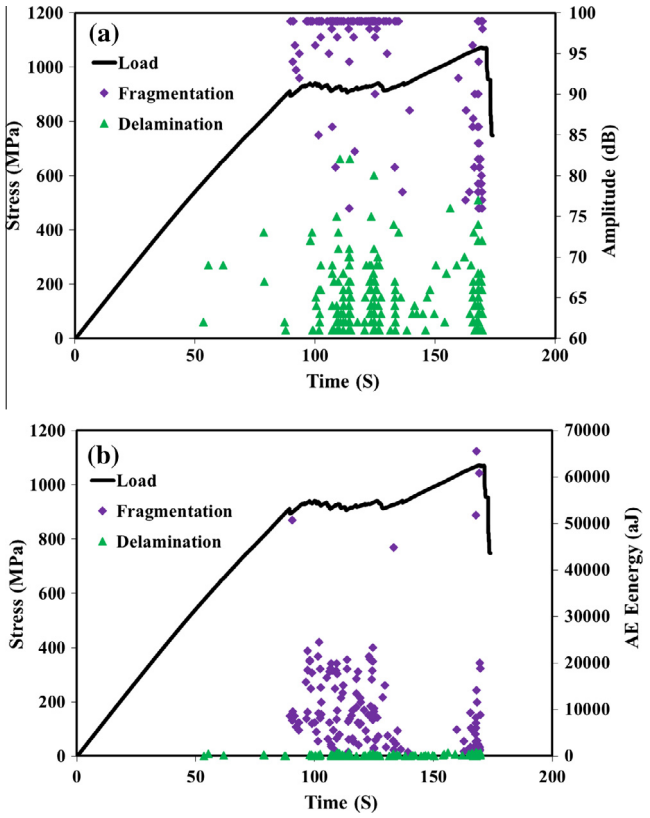

Fig. 12. Distribution of (a) amplitude and (b) energy of the AE events for a typical MR40/S-glass specimen. (For interpretation of the references to colour in this figure legend, the reader is referred to the web version of this article.)

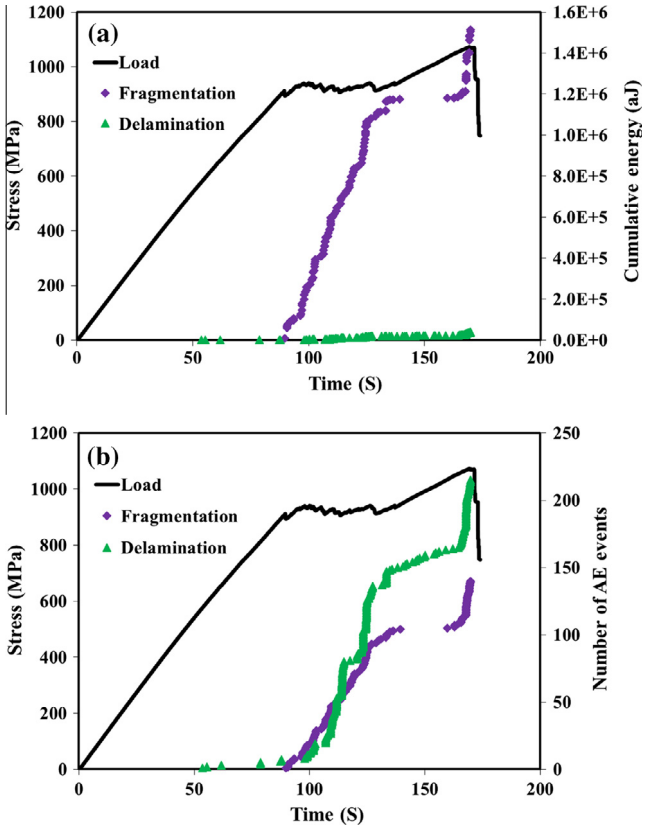

Fig. 13. The cumulative of (a) AE energy and (b) number of the AE events in each class of the AE signals in a typical MR40/S-glass specimen. (For interpretation of the references to colour in this figure legend, the reader is referred to the web version of this article.)

cut. The order of magnitude of the typical event energy in Fig. 6 is higher compared to Fig. 9, which is due to the high energies for the ply fragmentation. Also there were some weak AE signals from the start of the test with the amplitude <65 dB and energy <30 aJ which were not related to the delamination and considered as noise.

For the specimens without pre-cuts, the observed damage modes were correlated to the AE events obtained during the test. The correlation was based on the AE characteristics of the delamination and fragmentation, which led to grouping the AE events in two types. Based on our observation, two significant failure modes occurred during the tests. Ply fragmentation was associated with the high energy and amplitude range of the AE signals and delamination was related to the intermediate energy and amplitude range. The ranges of the AE energy and amplitude for the failure modes are indicated in Fig. 10a. These are the regions on the energy-amplitude plane, where damage mechanisms can be identified clearly. The proposed ranges for amplitude are not precise and there are some overlaps, but as can be seen from Fig. 10b, the density of the AE events in the overlapping areas is negligible.

The ranges for the energy and amplitude parameters introduced in Fig. 10a were used as filtering criteria to classify the damage mechanisms. This means that three different classes of signals can be identified: class (1) signals with 40–65 dB amplitude and 0–30 aJ energy related to noise, class (2) signals with 60–85 dB amplitude and 30–800 aJ energy related to the delamination of the carbon layer from the glass layer, class (3) signals with 75–100 dB amplitude and 800–65,000 aJ energy originating from fragmentation of the carbon plies. Fig. 11a shows all the obtained AE data for a typical MR40/S-glass hybrid specimen without applying any filtering condition defined in Fig. 10 whereas Fig. 11b shows the results after applying the filters. There were some AE signals out of the classified AE energy and amplitude ranges shown in Fig. 10a, but the percentage of them was very low so they were discarded, as clearly shown in Fig. 11a. The noise signals, with amplitude range 40–65 dB and energy range 0–30 aJ, were found to be less important and were not considered further.

Based on the classification results, the distribution of energy and amplitude of a typical MR40/S-glass specimen for the clustered signals is illustrated in Fig. 12.

It can be seen from Fig. 12 that the signals related to fragmentation appear from the second strain regime and they are well separated from those related to delamination. Most of the delamination related signals appear a bit later than the fragmentation ones. At the beginning of the third region number of high energy signals decreases which means that there is no more fragmentation of the carbon layer. Later near the maximum load, high amplitude, high energy signals re-appear which are related to fracture of the glass layer. The activity of delamination originated signals continues up to the final failure which is mainly because even after saturation of the carbon layer fragmentation, dispersed delamination were still growing. Some of these signals were also observed in the first region which must have been related to noise because there was no damage with a significant effect on the specimen's integrity in the linear-elastic region, as no change in the stiffness was observed.

The cumulative AE energy and number of the AE events in each class of signals are illustrated in Fig. 13, for a typical MR40/S-glass specimen. Fragmentation associated signals have much higher cumulative energy compared with the delamination associated ones. In addition, it is possible to count the number of failures in each class based on the number of AE events that hit the sensor.

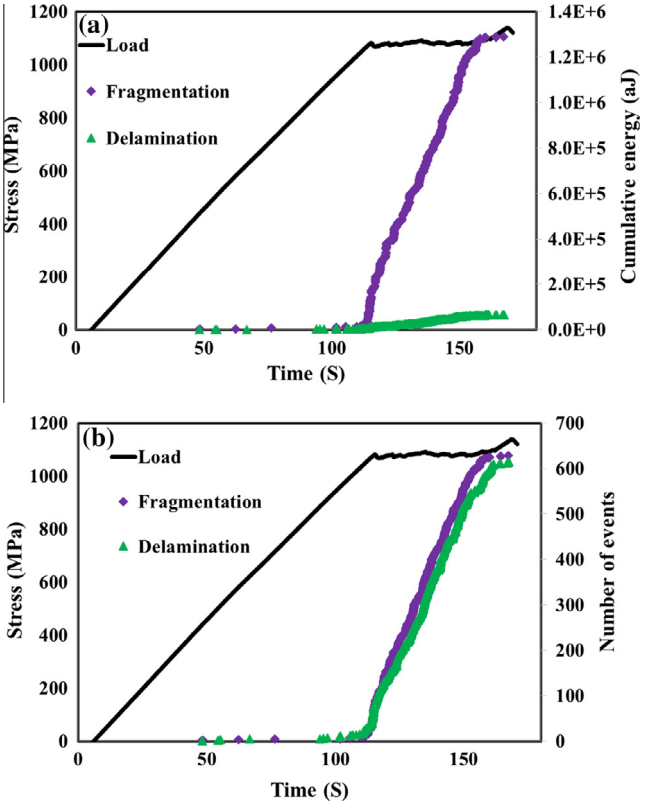

Fig. 14. The cumulative of (a) AE event energy and (b) number of the AE events in each class of the AE signals for a typical 2TR30/S-glass specimen with two carbon plies. (For interpretation of the references to colour in this figure legend, the reader is referred to the web version of this article.)

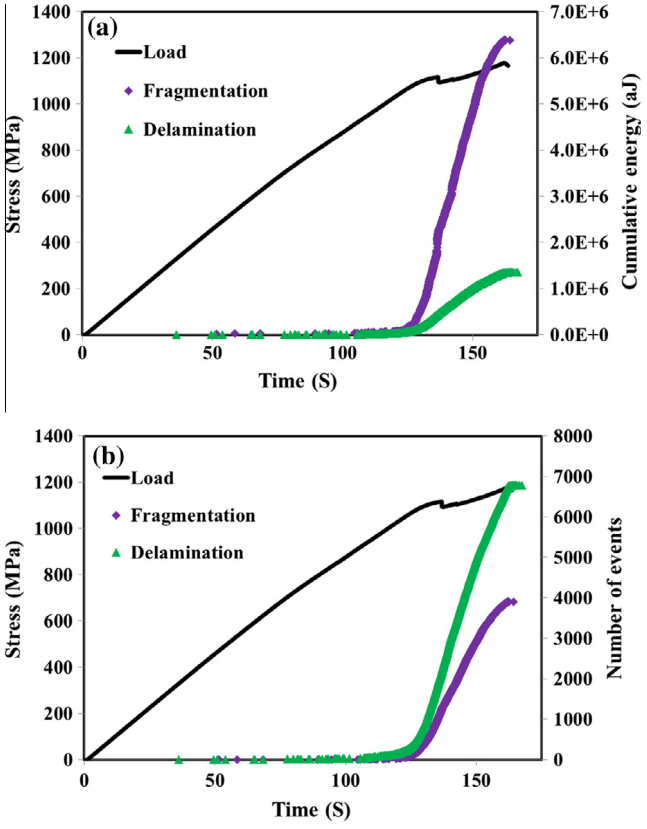

Fig. 15. The cumulative of (a) AE energy and (b) number of the AE events in each class of the AE signals for a typical 1TR30/S-glass specimen with one carbon ply. (For interpretation of the references to colour in this figure legend, the reader is referred to the web version of this article.)

An AE event is the phenomenon which releases elastic energy in the laminate, which then propagates as an elastic wave. In this case the mechanisms were either fragmentation or delamination and each AE signal can be regarded as a separate damage event. By visual counting the number of AE events on a typical specimen, the number of fragmentations in the carbon layer in MR40 is found to be about 105.

Using the same procedures introduced for MR40/S-glass, the cumulative AE energy and number of AE events in each class are illustrated in Figs. 14 and 15, for the 2TR30/S-glass and 1TR30/S-glass specimens with two and one carbon plies. The number of AE events related to fragmentation is 620 and 4000 for two layers and one layer of carbon, respectively. The number of AE events associated with delamination is also illustrated in the figures. For all the specimens, the delamination related signs and the fragmentation ones appear at about the same time.

These results are in good overall agreement with our visual inspection of the specimens and the videos captured during the tests. For the MR40/S-glass specimen type, it was easily possible to count the number of fragmentations and it was found to be around 100. Some images are shown for a typical MR40/S-glass specimen in Fig. 16. Some low magnification microscope images obtained from the surface of the different specimen types are shown in Fig. 17. The delaminated back surface of the glass layer blocked the visibility of the carbon. Therefore, the well bonded areas appear black, and within the locally delaminated light areas, the cracks in the carbon layer are visible as sharp bright lines, as highlighted in Fig. 16b. The bright lines within the light patches of local delamination are the fractures and the number of these lines is equal to the black lines. As the black lines are more visible, these were counted. There are some large black lines which go all across the width and other black lines which are shorter. Each separate black line (with different sizes) was counted as a ply fracture.

From our observation during the tests and as illustrated in Figs. 16 and 17, fragmentation and delamination occur concurrently, and are the origin of most of the AE signals. But the density and dispersion of these damage modes are different for the different specimen types. For MR40/S-glass the lowest number of fragmentations is observable and for 1TR30/S-glass, the number of fragmentations is highest. For MR40/S-glass the induced delamination size is bigger than for 2TR30/S-glass and 1TR30/S-glass specimen types, and the corresponding AE events in MR40/S-glass have a higher energy content compared with the smaller damage size and lower energy events in 2TR30/S-glass and 1TR30/S-glass. As indicated in Figs. 13–15, the number of fragmentation events prior to final failure is 104, 628 and 3907 and the average induced AE energy is about 1.175, 1.287 and 6.387 pJ, for MR40/S-glass, 2TR30/S-glass and 1TR30/S-glass, respectively, giving an average

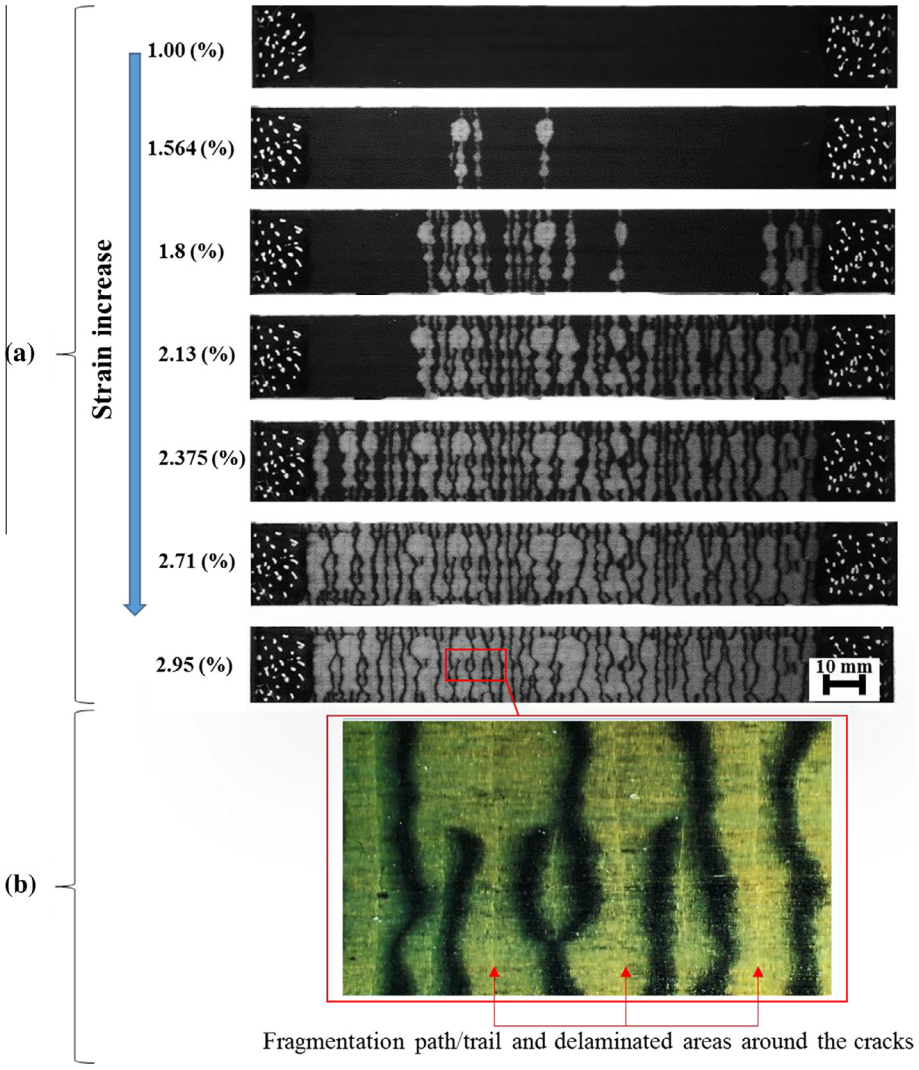

Fig. 16. (a) The appearance of a typical MR40/S-glass specimen at different strains during the tensile test and (b) Microscopy pictures with higher zoom (the fragmentation path and delaminated areas around the cracks). (For interpretation of the references to colour in this figure legend, the reader is referred to the web version of this article.)

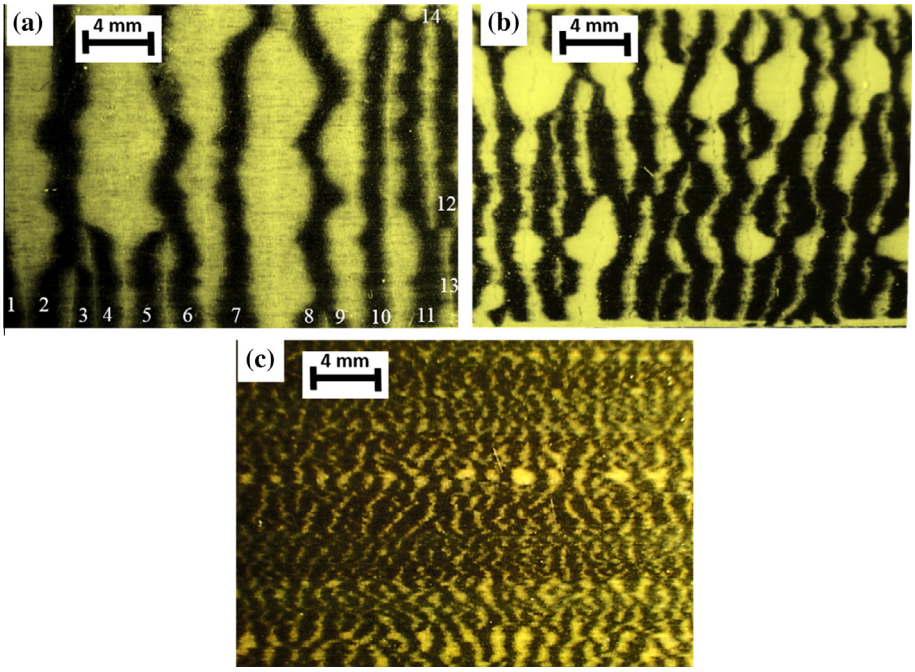

Fig. 17. Microscopic images from the surface of typical (a) MR40/S-glass, (b) 2TR30-S-glass and (c) 1TR30/S-glass. (For interpretation of the references to colour in this figure legend, the reader is referred to the web version of this article.)

Table 2
Number of ply fragmentations and energy content for the investigated layups.

Specimen type	Number of fragmentation events obtained by the AE	Average energy content for each fragmentation (aJ)
MR40	104	11,300
2TR30	628	2050
1TR30	3907	1635

energy content for fragmentation of 11,300, 2050 and 1635 aJ. The results are summarised in Table 2 for better comparison.

4. Conclusions

The number and order of the AE events in UD carbon/S-glass hybrid laminates under tensile loading were correlated to direct observations of fragmentation and delamination during loading. The correlation was based on the AE characteristics, which led to grouping the AE events into two types. The high and low values of energy and amplitude were associated with fragmentation of carbon plies and delamination of the glass/carbon interface, respectively. Since the laminates were translucent it was possible to establish quantitative correlations between the observed failures and the AE events during the tests especially for the MR40/S-glass specimen type. In addition, the cumulative numbers of the AE signals were used to monitor the damage evolution in the specimens. It is concluded that the proposed method is a simple and strong tool to characterise the failure mechanisms in hybrid laminates and can be used for detection of damage initiation, as well as subsequent tracking of its evolution, especially where the laminates are opaque, thicker or of more complex geometry where it is not possible to monitor the damage evolution visually.

Acknowledgements

This work was funded under the UK Engineering and Physical Sciences Research Council Programme Grant EP/I02946X/1 on High Performance Ductile Composite Technology in collaboration with Imperial College, London. Gergely Czél acknowledges the Hungarian Academy of Sciences for funding through the Post-Doctoral Researcher Programme fellowship scheme and the János Bolyai scholarship. The authors acknowledge Hexcel Corporation for supplying materials for this research. Supporting data can be requested from the corresponding author.

References

[1] Bunsell AR, Harris B. Hybrid carbon and glass fibre composites. Composites 1974;5:157–64.
[2] Summerscales J, Short D. Carbon fibre and glass fibre hybrid reinforced plastics. Composites 1978;9:157–66.
[3] Aveston J, Sillwood JM. Synergistic fibre strengthening in hybrid composites. J Mater Sci 1976;11:1877–83.
[4] Manders PW, Bader MG. The strength of hybrid glass/carbon fibre composites. J Mater Sci 1981;16:2233–45.
[5] Swolfs Y, Gorbatikh L, Verpoest I. Stress concentrations in hybrid unidirectional fibre-reinforced composites with random fibre packings. Compos Sci Technol 2013;85:10–6.
[6] Swolfs Y, Gorbatikh L, Verpoest I. Fibre hybridisation in polymer composites: a review. Compos A Appl Sci Manuf 2014;67:181–200.
[7] Czél G, Wisnom MR. Demonstration of pseudo-ductility in high performance glass-epoxy composites by hybridisation with thin-ply carbon prepreg. Compos A Appl Sci Manuf 2013;52:23–30.
[8] Czél G, Jalalvand M, Wisnom MR. Design and characterisation of advanced pseudo-ductile unidirectional thin-ply carbon/epoxy–glass/epoxy hybrid composites. Compos Struct, in preparation.
[9] Wisnom MR, Czél G, Swolfs Y, Jalalvand M, Gorbatick L, Verpoest I. Hybrid effects in thin ply carbon/glass unidirectional laminates: accurate experimental determination and prediction, Compos A Appl Sci Manuf, in preparation.
[10] Jalalvand M, Czél G, Wisnom MR. Numerical modelling of the damage modes in UD thin carbon/glass hybrid laminates. Compos Sci Technol 2014;94:39–47.
[11] Jalalvand M, Czél G, Wisnom MR. Damage analysis of pseudo-ductile thin-ply UD hybrid composites – a new analytical method. Compos A Appl Sci Manuf 2015;69:83–93.
[12] Jalalvand M, Czél G, Wisnom MR. Parametric study of failure mechanisms and optimal configurations of pseudoductile thin-ply UD hybrid composites. Compos A Appl Sci Manuf 2015;74:123–31.
[13] Fuller JD, Jalalvand M, Wisnom MR. Combining fibre rotation and fragmentation to achieve pseudo-ductile CFRP laminates. Compos Struct 2016;142:155–66.
[14] Ronnie KM. Handbook of nondestructive testing, Vol. 5. Acoustic emission. 2nd ed. American Society for Nondestructive Testing; 1987.

[15] Siron O, Chollon G, Tsuda H, Yamauchi H, Maeda K, Kosaka K. Microstructural and mechanical properties of filler-added coal-tar pitch-based C/C composites: the damage and fracture process in correlation with AE waveform parameters. Carbon 2001;39:2065–75.
[16] Ramirez-Jimenez CR, Papadakis N, Reynolds N, Gan T, Purnell P, Pharaoh M. Identification of failure modes in glass/polypropylene composites by means of the primary frequency content of the acoustic emission event. Compos Sci Technol 2004;64:1819–27.
[17] Pashmforoush F, Khamedi R, Fotouhi M, Hajikhani M, Ahmadi M. Damage classification of sandwich composites using acoustic emission technique and k-means genetic algorithm. J Nondestr Eval 2014;33:481–92.
[18] Fotouhi M, Ahmadi M. Acoustic emission based study to characterize the initiation of mode I delamination in composite materials. J Thermoplast Compos Mater 2014. http://dx.doi.org/10.1177/0892705713519811.
[19] Arumugam V, Sidharth AAP, Santulli C. Failure modes characterization of impacted carbon fibre reinforced plastics laminates under compression loading using acoustic emission. J Compos Mater 2014;48(28):3457–68.
[20] Barré S, Benzeggagh ML. On the use of acoustic emission to investigate damage mechanisms in glass-fibre-reinforced poly-propylene. Compos Sci Technol 1994;52(3):369–76.
[21] Benmedakhene S, Kenane M, Benzeggagh ML. Initiation and growth of delamination in glass/epoxy composites subjected to static and dynamic loading by acoustic emission monitoring. Compos Sci Technol 1999;59:201–8.
[22] Bohse J. Acoustic emission characteristics of micro-failure processes in polymer blends and composites. Compos Sci Technol 2000;60(8):1213–26.
[23] Guerjouma RE, Baboux JC, Ducret D, Godin N, Guy P, Huguet S, et al. Nondestructive evaluation of damage and failure of fiber reinforced polymer composites using ultrasonic waves and acoustic emission. Adv Eng Mater 2001;3:601–8.
[24] Woo SC, Choi NS. Analysis of fracture process in single-edge-notched laminated composites based on the high amplitude acoustic emission events. Compos Sci Technol 2007;67:1451–8.
[25] Palazzetti R, Zucchelli A, Gualandi C, Focarete ML, Donati L, Minak G. Influence of electrospun Nylon 6,6 nanofibrous mats on the interlaminar properties of Gr–epoxy composite laminates. Compos Struct 2012;94(2):571–9.
[26] Fotouhi M, Ahmadi M. Investigation of the mixed-mode delamination in polymer-matrix composites using acoustic emission technique. J Reinf Plastic Comp 2014;33(19):1767–82.
[27] Lomov SV, Bogdanovich AE, Ivanov DS, Mungalov D, Karahan M, Verpoest I. A comparative study of tensile properties of non-crimp 3D orthogonal weave and multi-layer plain weave E-glass composites. Part 1: Materials, methods and principal results. Compos A Appl Sci Manuf 2009;40:1134–43.
[28] Fotouhi M, Pashmforoush F, Ahmadi M, Refahi A. Monitoring the initiation and growth of delamination in composite materials using acoustic emission under quasi-static three-point bending test. J Reinf Plast Compos 2011;30:1481–93.
[29] Suresh Kumar C, Arumugam V, Dhakal HN, John Risil. Effect of temperature and hybridisation on the low velocity impact behavior of hemp-basalt/epoxy composites. Compos Struct 2015;125:407–16.
[30] Godin N, Huguet S, Gaertner R, Salmon L. Clustering of acoustic emission signals collected during tensile tests on unidirectional glass/polyester composite using supervised and unsupervised classifiers. NDT and E Int 2004;37:253–64.
[31] Godin N, Huguet S, Gaertner R. Integration of the Kohonen's self-organising map and k-means algorithm for the segmentation of the AE data collected during tensile tests on cross-ply composites. NDT and E Int 2005;38:299–309.
[32] Pashmforoush F, Fotouhi M, Ahmadi M. Acoustic emission-based damage classification of glass/polyester composites using harmony search k-means algorithm. J Reinf Plastic Comp 2012;31:671–80.
[33] Zarif Karimi N, Heidary H, Ahmadi M. Residual tensile strength monitoring of drilled composite materials by acoustic emission. Mater Design 2012;40:229–36.
[34] Fotouhi M, Saeedifar M, Sadeghi S, Ahmadi M, Minak G. Investigation of the damage mechanisms for mode I delamination growth in foam core sandwich composites using Acoustic Emission. Struct Health Monit 2015. http://dx.doi.org/10.1177/1475921714568403.
[35] Al-Jumaili SK, Holford KM, Eaton M, McCrory J, Pearson MR, Pullin R. Classification of acoustic emission data from buckling test of carbon fibre panel using unsupervised clustering techniques. Struct Health Monit 2015;14(3):241–51.
[36] Li L, Lomov S, Yan X. Correlation of acoustic emission with optically observed damage in a glass/epoxy woven laminate under tensile loading. Compos Struct 2015;123:45–53.
[37] Huang M, Jiang L, Liaw PK, Brooks ChR, Seeley R, Klarstrom DL. Using acoustic emission in fatigue and fracture materials research. Nondestruct Eval Overview 1998;50:11.
[38] Minak G, Abrate S, Ghelli D, Panciroli R, Zucchelli A. Low-velocity impact on carbon/epoxy tubes subjected to torque–experimental results, analytical models and FEM analysis. Compos Struct 2010;92(3):623–32.
[39] Fotouhi M, Sadeghi S, Jalalvand M, Ahmadi M. Analysis of the damage mechanisms in mixed-mode delamination of glass/epoxy composites using acoustic emission data clustering. J Thermoplast Compos Mater 2015. http://dx.doi.org/10.1177/0892705715598362.